ACADEMIC PRESS

Available online at www.sciencedirect.com

SCIENCE DIRECT®

Journal of Sound and Vibration 265 (2003) 841–861

JOURNAL OF SOUND AND VIBRATION

www.elsevier.com/locate/jsvi

Validation of a medium-frequency computational method for the coupling between a plate and a water-filled cavity

J.-M. David*, M. Menelle

Structural Dynamics and Coupled Systems Department, ONERA, 29 Avenue de la Division Leclerc, 92322 Châtillon cedex, France

Received 29 May 2002; accepted 12 August 2002

Abstract

The aim of this paper is the validation of a computation by a numerical method, normally adapted to the medium-frequency (MF) domain, of the strong coupling between an elastic structure (plate) and a cavity entirely filled with an internal acoustic viscous dense fluid (water). The method of computation does not lie in a modal approach (no need to extract the modal basis of the system) but it directly computes the frequency response of the system using a specific algorithm called the ''Onera-MF method''.

This method was developed to accurately calculate the response of complex systems in an MF broad band at a lower cost than standard modal method or direct step-by-step frequency method. The method can also be used for the low-frequency (LF) domain where modal densities of systems are low. The computation of the vibroacoustic response of the system lies in a finite element modelling of the overall system (structure and fluid) in which the coupling between the structure and the fluid (light or heavy) is directly taken into account within the formulation of the finite elements.

A simple and well-known experimental case was chosen for validation: a parallelepipedic cavity entirely filled with water contained in a box defined by five rigid faces and closed at its end by an elastic clamped homogeneous plate.

The validation is based on a comparison between measurement, the numerical computation and an analytical approach in the frequency band [0, 5000 Hz]. Both the vibratory response of the plate and the acoustic pressure were compared. This study shows that the MF-method of computation used herein for this case also works in a modal domain.

*Corresponding author. Fax: +33-1-46-7341-43.
E-mail address: jean-michel.david@onera.fr (J.-M. David).

0022-460X/03/$ - see front matter
doi:10.1016/S0022-460X(02)01529-8

1. Introduction

The aim of this work is to present a case of validation for the coupling of an elastic plate with an acoustic cavity filled with water in the frequency band [0, 5000 Hz].

In the first step, the vibroacoustic response of the system was measured. The cavity was firstly open and the effect of the clamping on the dynamics of the plate was analyzed. Then the cavity was filled with water and the hydroelastic coupling between the plate and a dense fluid was studied.

In the second step, a numerical computation has been carried out.

Even though this kind of work has already been performed by several previous authors, the originality of the present work lies in the following facts:

- Firstly, we are able to measure accurately the vibratory response and the internal acoustic pressure in water of a quite small system in a large frequency band.
- Secondly, for the numerical computation, we never used a modal reduction approach nor a direct step-by-step frequency method. We used a specific method called the ''Onera-MF method'' which normally suits a frequency domain where the analyzed systems have a medium-frequency (MF) (non-modal) behaviour.

In the present case, the results of the test campaign on the vibroacoustic response of the system exhibit a modal (not a mid-frequency) behaviour in the analyzed frequency band due to the fact that the size of the structure is small and that the modal density is fairly poor. But the MF-method used herein also works for this case of modal behaviour at a smaller cost compared to the cost of a standard modal approach or of a direct step-by-step frequency method. This method of ''two time scales'', based on the use of a time integration and a Fourier-transform-type technique, directly calculates the vibroacoustic response of the system in the frequency domain without having to extract the modal basis of the overall system before calculating the response.

An analytical method, based on a modal approach, was also developed in order to validate both the measurements and the numerical computation.

2. Description of the analyzed vibroacoustic system

A steel elastic homogeneous plate which is 170 mm long, 150 mm broad and 4 mm thick, is clamped by its four edges on a massive box shaped from a 320 mm steel cylinder (see Figs. 1 and 2). The plate was fixed and blocked up at the top of the rigid box with a 30 mm thick plate and by a row of 20 bolts as shown in Fig. 3. The bottom of the box was also blocked up with a 30 mm thick plate in order to obtain a parallelepipedic cavity of 310 mm height, which has five infinitely rigid faces up to a frequency of about 5000 Hz and one elastic face which is constituted by the plate. The size of the box (which is small) was chosen to minimize the mass of the structure (about 150 kg) and make the handling of the box easier for the test. A second reason of the smallness of the system is that this structure was initially sized for another purpose than a vibroacoustic analysis.

The plate is excited by one mechanical force on a point as shown in Fig. 2.

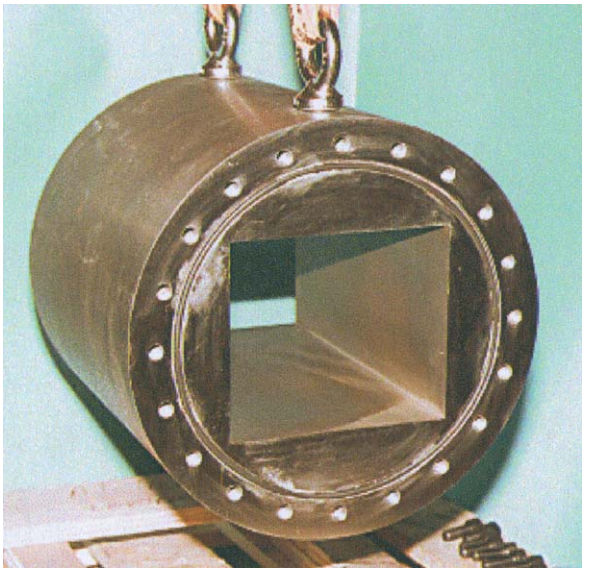

Fig. 1. View of the test structure and the cavity.

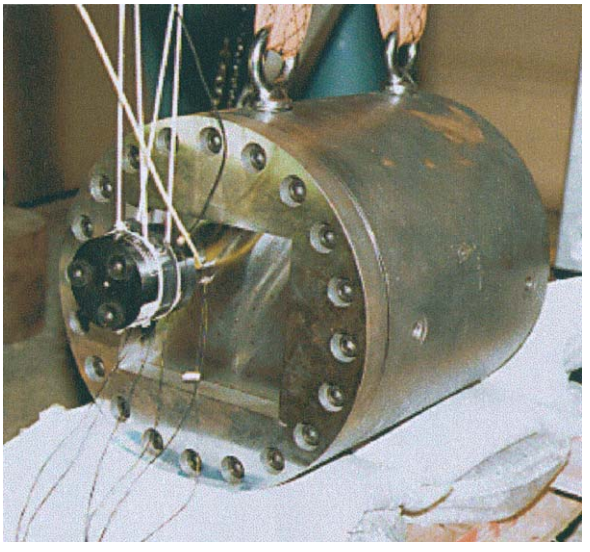

Fig. 2. Implementation of plate clamping and force exciter.

3. Experiments

3.1. Instrumentation

Bruel&Kjaer 4374 low-mass accelerometers are used for the measurement of vibrations of the plate. Plate length and width are divided into 10 parts and this leads to 121 locations as shown in Fig. 4 in order to obtain precisely its modal forms.

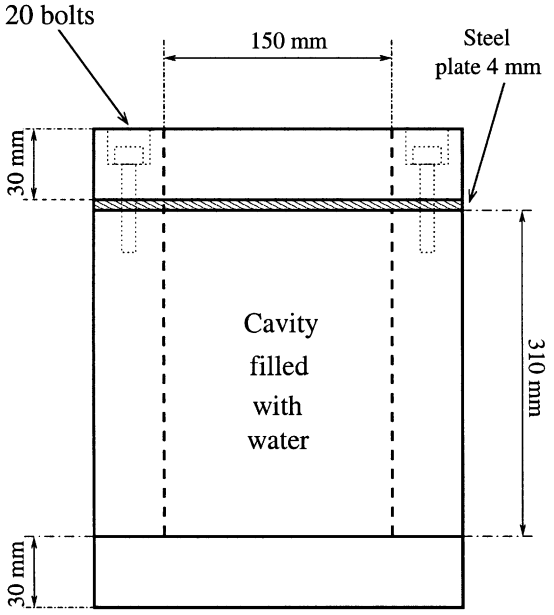

Fig. 3. Simplified description of the plate clamping into the rigid box.

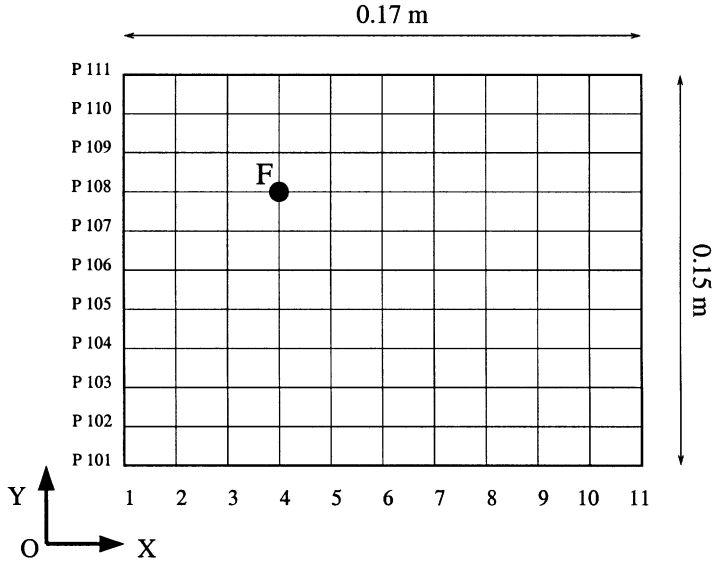

Fig. 4. Plate meshing of accelerometers used to identify modal forms.

A Bruel&Kjaer 4810 electrodynamic exciter and a force cell, developed at ONERA, are used for exciting the plate. The force sensor which is suitable for light structures has a parasitic mass of less than 0.5 g.

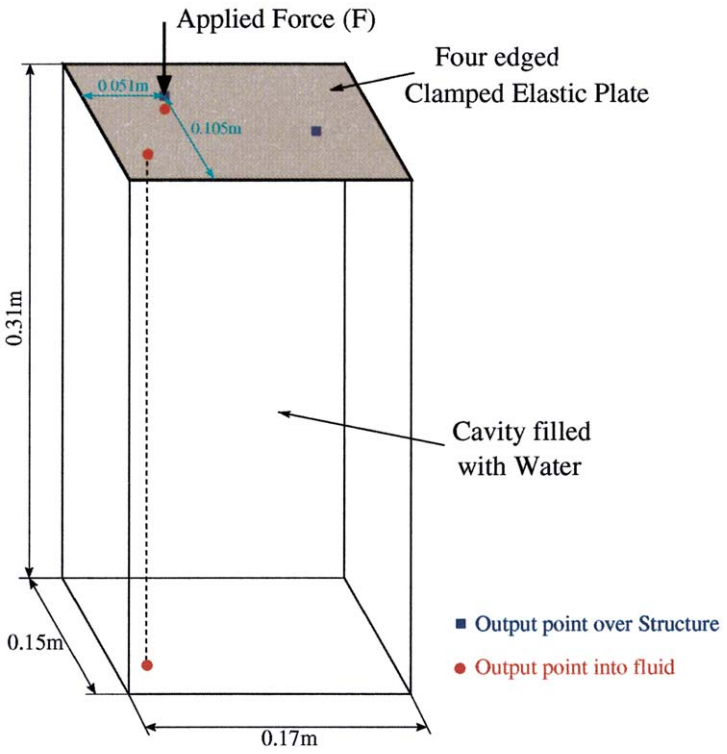

Fig. 5. Description of the analyzed vibroacoustic system and selection of measurement points.

An ENTRAN EPL-B02 pressure sensor is located at the end of a tube and is inserted inside the cavity by holes made at its back, when the cavity is filled with water. The pressure was measured under the excitation point and on a vertical line under (20 mm, 20 mm) structural point as shown in Fig. 5.

3.2. Measurements

The measurement hardware is composed of a front-end device SCADAS II from DIFA and of an HP B160L workstation which makes a Leuven Measurement System (LMS) run.

The exciter is supplied with a stationary random signal for vibrating the structure. Six accelerometers are moved to all locations on the plate and the frequency response functions (FRF) of the structure are measured using an H1 estimator.

A blocksize of 16 384 was used which leads to a frequency resolution of 1.221 Hz up to the frequency of 10 kHz.

In the first step, the box is open and a modal analysis using LMS software is performed to obtain the in vacuo eigenmodes and eigenfrequencies of the clamped plate. The application specific monitor used was the "time-domain multi-degrees of freedom". The measured transfer response function at the excitation point and an analytical calculation based on results given in Ref. [1] are compared in Fig. 6. The best fit of the two curves is obtained by using for the plate a

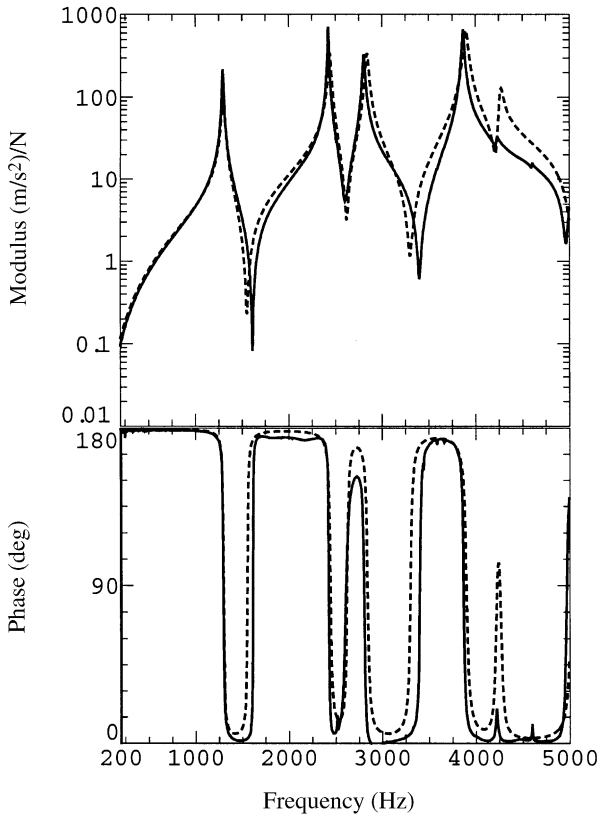

Fig. 6. Comparison of theoretical and experimental FRF at excitation point for the plate in vacuo.

Young's modulus of 1.715×10^{11} Pa. The 18% gap with respect to the real value of 2.1×10^{11} Pa is due to the imperfect clamping of the plate because, as a matter of fact, the steel plate is fixed on a frame made up of the same material.

The phase value included between 0° and 180° shows the efficiency of the force cell. In fact, the positive power input into a system implies that the real part of the transfer function (FRF) between force and velocity at excitation point is positive. This means that the imaginary part of the FRF between force and acceleration is positive and consequently the phase must be included between 0° and 180° as shown in Fig. 6.

The LMS software also provides the calculation of the modal assurance criterion (MAC) which tests the linear dependence between two modes. MAC is defined as

$$MAC_{ij} = \frac{\{\boldsymbol{\phi}_i^T \boldsymbol{\phi}_j\}^2}{\{\boldsymbol{\phi}_i^T \boldsymbol{\phi}_i\} \cdot \{\boldsymbol{\phi}_j^T \boldsymbol{\phi}_j\}}, \tag{1}$$

where $\boldsymbol{\phi}_i$ and $\boldsymbol{\phi}_j$ are modal forms of real eigenmodes i and j.

The MAC is used for the comparison of a set of modes between each other or for the correlation of two different sets [2,3]. It can also compare measured modes to predicted modes or measured modes of a structure in different states.

Table 1
MAC calculation of the first five modes in vacuo

Frequencies (Hz)	Measured modes				
	1293.	2424.	2804.	3866.	4224.
Measured modes					
1293.	**100.**				
2424.	0.3	**100.**			
2804.	0.0	0.3	**100.**		
3866.	0.0	0.6	0.1	**100.**	
4224.	0.2	0.1	0.1	0.6	**100.**
Computed modes					
1290.	**99.5**	0.2	0.0	0.0	0.7
2428.	0.0	**98.2**	0.2	0.1	0.0
2825.	0.0	0.0	**97.7**	0.1	0.1
3878.	0.0	0.2	0.0	**95.7**	0.7
4237.	0.1	0.2	0.0	0.0	**95.3**

Table 2
Correlation between measured frequencies for plate coupled to water and measured frequencies for plate in vacuo and *MAC* calculation

Frequencies (plate coupled to water) (Hz)	In vacuo				
	Type (1,1), 1293. Hz	Type (2,1), 2424. Hz	Type (1,2), 2804. Hz	Type (2,2), 3866. Hz	Type (3,1), 4224. Hz
1129.	**99.8**	0.5	0.0	0.0	0.1
1654.	0.0	**97.2**	0.2	0.0	0.1
1952.	0.0	0.0	**99.2**	0.2	0.1
2687.	**63.3**	0.5	0.1	2.2	**33.7**
2908.	0.0	0.5	0.0	**99.1**	0.8
3386.	0.5	0.1	0.1	0.4	**96.5**

Table 1 shows the calculation of the *MAC* of the first five measured and computed modes with regard to the measured modes. We can note that the shape of measured modes is very close to the one of theoretical modes of a perfect clamped plate. These results also show the quasi-perfect orthogonality of the measured modes.

After the modal identification of the system in vacuo and the updating of plate clamping on the rigid cylinder, the box was filled with water and closed. The transfer response functions between accelerometers and force for the plate and between pressure sensors and force for the cavity were measured and an identification of first resonant frequencies for plate coupled to water was performed afterwards.

Table 2 shows the correlation between measured frequencies when the plate is coupled to water and measured frequencies for plate in vacuo and the *MAC* calculation. We can note that

eigenfrequencies of modes for plate in vacuo are shifted by a factor included between 0.6 and 0.8 when the plate is coupled to water due to the effect of added mass of water acting on the plate. This result expresses a strong coupling between the plate and the cavity when it is filled with water. In the list of frequencies due to coupled modes (given in Table 2), the fourth one at 2687 Hz comes from the coupling of the first acoustic mode of cavity with rigid walls (which is located at 2420 Hz) and the first and fifth modes of the plate in vacuo (located at 1293 and 4224 Hz).

Experimental results will be now compared to analytical and numerical simulations.

4. Numerical and analytical simulations

4.1. Numerical computation

A computation by the finite element method was performed on the system in order to predict the internal noise and vibration levels in band [0, 5000 Hz].

A finite element modelling of the overall structure was developed. The model is adapted to the analyzed frequency band in terms of the size of elements.

- This model was developed using the I-deas meshing software.
- The computation was performed using the "In-house" finite element software named Adina–Onera in which we have implemented a specific method called the "*Onera-MF method*" [4–6].

Before introducing the MF-method used for the numerical approach, we are going to describe the general formulation of the vibroacoustic problem to be solved.

4.1.1. Expression of the coupling between an acoustic bounded fluid and an elastic structure

The coupling between an internal acoustic fluid and an elastic structure is expressed in terms of the couple $(\mathbf{u}, \Phi)$, where $\mathbf{u}$ is the unknown displacement field of the structure and Φ the velocity potential within the fluid.

The weak final formulation of the two coupled domains is given in time domain under the form of operators by the following expression:

$$\begin{bmatrix} \mathbf{M} & 0 \\ 0 & -\mathbf{Q} \end{bmatrix} \begin{pmatrix} \dfrac{\partial^2 \mathbf{u}}{\partial t^2} \\ \dfrac{\partial^2 \Phi}{\partial t^2} \end{pmatrix} + \begin{bmatrix} \mathbf{C} & \mathbf{H} \\ \mathbf{H}^t & -\dfrac{4}{3}\dfrac{\eta_0}{\rho_0 c_0^2}\mathbf{R} \end{bmatrix} \begin{pmatrix} \dfrac{\partial \mathbf{u}}{\partial t} \\ \dfrac{\partial \Phi}{\partial t} \end{pmatrix} + \begin{bmatrix} \mathbf{K} & 0 \\ 0 & -\mathbf{R} \end{bmatrix} \begin{pmatrix} \mathbf{u} \\ \Phi \end{pmatrix} = \begin{pmatrix} \mathbf{G} \\ 0 \end{pmatrix}. \tag{2}$$

The above operators $\mathbf{M}$, $\mathbf{Q}$, $\mathbf{C}$, $\mathbf{H}$, $\mathbf{R}$, $\mathbf{K}$ and $\mathbf{G}$ are defined in Appendix A and $(\mathbf{u}, \Phi)$ formulation used herein is given in full detail in the book [7, Chapter 8].

We can see that the coupling between the two systems is a *coupling by damping* and is due to operator $\mathbf{H}$. From a practical point of view, the coupling between elements for the structure and elements for the fluid will be carried out by introducing an element of interface.

Expression (2) of the vibroacoustic problem has three main advantages:

1. it is symmetric and nodes of fluid elements have only one degree of freedom (d.o.f.) which is a potential scalar,

2. it takes into account the viscous dissipation of the fluid and
3. it is very well-adapted for the Onera-MF method because this equation of coupling can be put under the general form

$$\mathbf{M}\ddot{\mathbf{u}}(t) + \mathbf{C}\dot{\mathbf{u}}(t) + \mathbf{K} = \mathbf{f}(t). \tag{3}$$

In terms of operators discretized by finite element method in the frequency domain, the linear real matrices system to be solved is then

$$[-\omega^2\mathbf{M} + \mathrm{j}\omega\mathbf{C}(\omega) + \mathbf{K}(\omega)]\hat{\mathbf{u}}(\omega) = \hat{\mathbf{f}}(\omega). \tag{4}$$

This general matrix system can be solved directly in frequency domain by a mixed method of "two time scales" called the "*Onera-MF method*".

4.1.2. Characteristics of medium-frequency domain

MF-domain is the frequency domain where modal densities of systems are not constant. They can be either high or poor when frequency is varying within the analyzed band. In this domain, characteristics of materials can vary with frequency and in that case it is not possible to find a unique conservative system associated to the analyzed system within a large range of frequencies. Moreover, finite element meshings used for the resolution in this frequency band must be built using a large number of nodes and consequently a large number of d.o.f.'s; which leads to handling large-matrices systems.

That is why standard methods of modal reduction usually used in low-frequency (LF) domain are not accurate when frequency increases. The use of such methods requires to extract a very high number of eigenmodes of the vibroacoustic system, at prohibitive cost and without assuming convergence of iterative algorithms.

A direct frequency-by-frequency method is also not envisaged at a reasonable numerical cost because we have to inverse at each discrete frequency a very-large-matrices complex system (4) having a very high number of physical d.o.f.'s.

4.1.3. Onera-MF method

The Onera-MF method is a numerical method of "two time scales" and it is based on the use of a time integration scheme coupled to a Fourier-transform-type technique.

A summary of the method is presented in Appendix B. For more details about this method, the reader is invited to see Ref. [4].

This method has been implemented in the Adina–Onera software where we were forced to complexify all matrices of finite element discretization and vectors of solution. The method has already been applied to many previous vibroacoustic problems in the MF-band. The main applications on more complex systems are given in Refs. [8–13].

4.1.4. Finite element model developed for the coupled system

The finite element model of the overall structural acoustic system used for the numerical computation is presented below.

- The meshing of the elastic plate uses $27 \times 24 \times 2$ classical *three-node-plate* elements contained in the Adina–Onera software.

- The acoustic fluid is meshed by $27 \times 24 \times 2 \times 25$ *six-node-3D-viscous fluid* elements which are also implemented in Adina–Onera.
- The six faces of the box (elastic and infinitely rigid) are meshed using 5142 *three- or four-node-2D-interface* elements. This element enables to build operator H.

The overall model has about **20 000** d.o.f'.s: 18 000 for the fluid (1 d.o.f. of potential per node) and 1 794 for the structure (3 d.o.f'.s of flexure per node).

4.1.5. Damping parameters introduced

- The mean structural damping factor denoted η_s and introduced for the structure was taken at a constant value of **0.8%** over the whole frequency band [0, 5000 Hz]. This value represents the averaged value of structural damping measured for each mode during the LF identification of the first modes of the plate in vacuo.
- The mean acoustic dissipation factor denoted η_a and introduced for the internal fluid is estimated from the data of its dynamical viscosity η_0 and it depends on the frequency as follows:

$$\eta_a(\omega) = \frac{4}{3}\frac{\eta_0}{\rho_0 c_0^2}\omega. \tag{5}$$

The above equation is obtained from the imaginary part within the formulation of the internal dissipation of the acoustic fluid as it is defined in the book [14, Chapter X, Section 3]. Values taken for ρ_0, c_0 and η_0 in Eq. (5) are: 1000 kg/m^3, 1500 m/s and 0.001 kg/m · s), respectively, when the internal fluid is water.

4.1.6. Numerical computation

The frequency band for the computation is the band [460, 5000 Hz] with a step of resolution of 1 Hz. The MF-method needs this frequency band be divided into 29 sub-bands.

The numerical calculation was carried out using the Adina–Onera software.

The selected points chosen for the comparisons are those defined in Fig. 5: two points over the plate and three points within the fluid.

The quantities observed are the FRFs $|\gamma(\omega)/F|$ for the structural points and $|P(\omega)/F|$ for the fluid points.

4.2. Analytical simulation

The analytical approach used in the simulations is entirely developed in Appendix C and it is based on results of the book [15].

5. Results and comparisons

The results obtained by the two simulations are now compared to measurements.

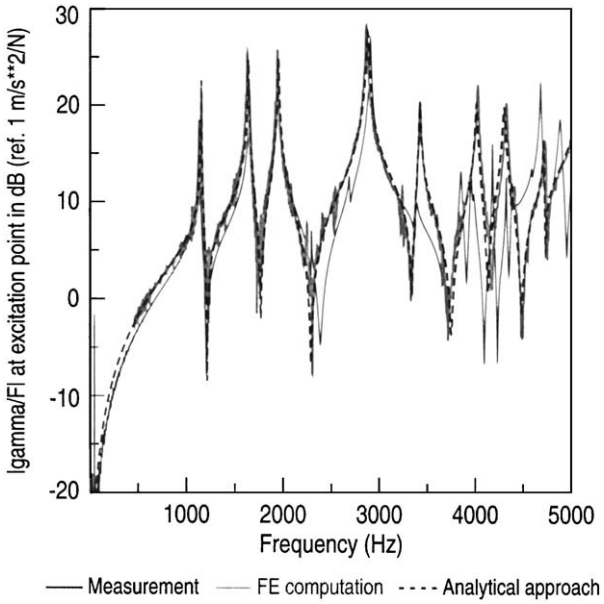

Fig. 7. Comparison of vibratory levels at excitation point (P108-4).

We can see in Figs. 7 and 8 the comparison for quantity $|\gamma(\omega)/F|$.
In Figs. 9–11, we can see the comparison for quantity $|P(\omega)/F|$.

6. Discussion

The analytical approach and the finite element computation are in perfect agreement on the whole frequency band. Compared to measurements, the two predictive curves fit well to measurement up to the frequency 3500 Hz. But from this frequency, we can see the notable influence of the plate clamping which becomes more and more imperfect when frequency is still increasing. The imperfection of the clamping is due to the fact that the steel plate is fixed in the box by a frame made up with the same material, which makes the clamping be more flexible. Another possible explanation could come from the following: (1) when pressure measurements are being done, the tube containing pressure sensors inserted into the cavity can move, (2) when we insert the tube into the cavity, a static over-pressure is created, which also creates a curvature to the plate and consequently modifies the dynamics of the plate.

The FRFs obtained on this hydro-elasto-acoustic system show a modal behaviour of the plate and consequently of the vibroacoustic system in the analyzed frequency band because modal densities are quite small due to the smallness of the structure. However, the numerical method used herein (which is normally adapted for an MF behaviour of systems) works. This method has the advantage of being globally cheaper than the standard modal reduction method or the direct frequency-by-frequency method and further the strong coupling between the structural element and the dense fluid is directly taken into account within the finite element formulation.

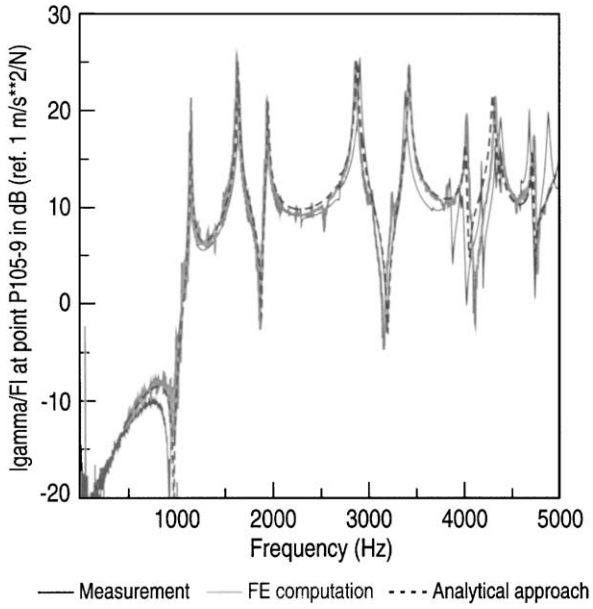

Fig. 8. Comparison of vibratory levels at point P105-9.

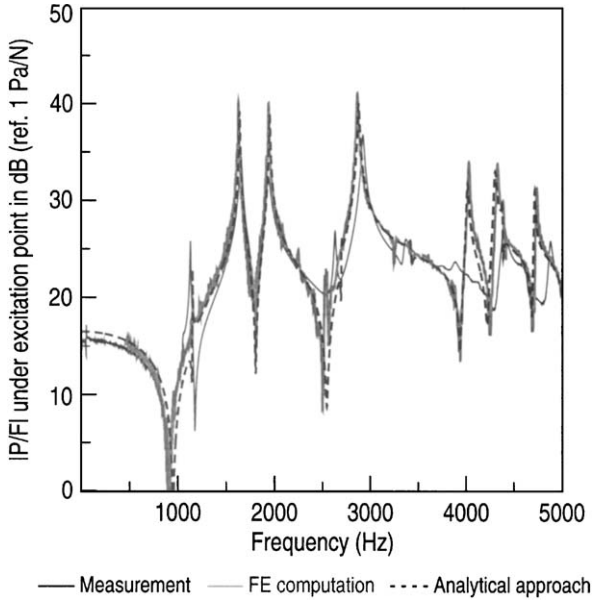

Fig. 9. Comparison of acoustic pressure levels inside fluid for point under excitation point.

7. Conclusion

Independent of the problem of the imperfect plate clamping into the box, measurements done on this vibroacoustic system are very well-controlled.

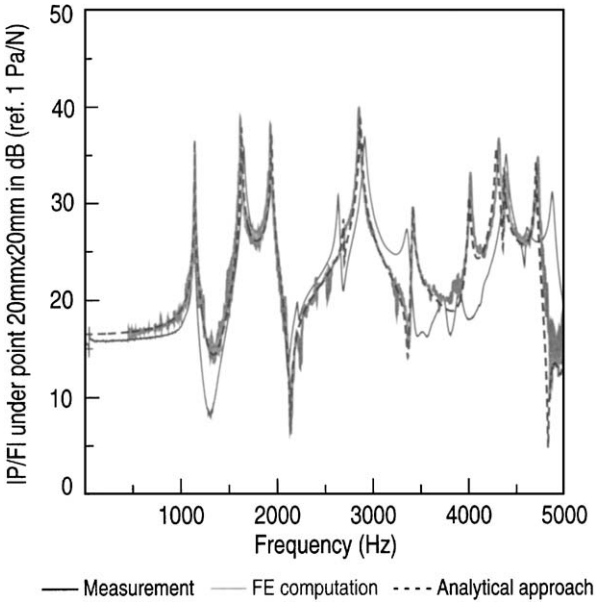

Fig. 10. Comparison of acoustic pressure levels inside fluid for point under structural point (20 mm, 20 mm).

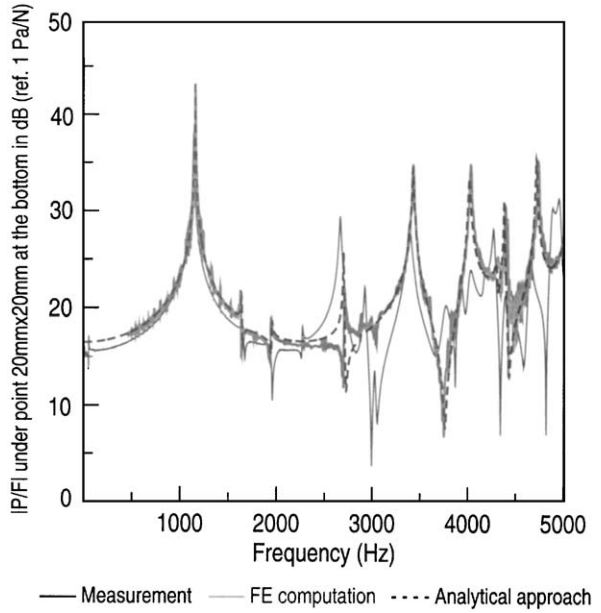

Fig. 11. Comparison of acoustic pressure levels inside fluid for point under structural point (20 mm, 20 mm) but in the bottom of box.

Considering the size of the box (small box), it is indeed difficult to build a perfect clamping for a small plate into a non-infinitely rigid box of the same material. That is why, an updating of the dynamics of the plate without water was carried out in a first step.

For the hydroelastic system, numerical computation and measurement fit well up to 3500 Hz without using any new approximation or updating the system. Numerical method and analytical method fit well on the whole analyzed frequency band.

The numerical method by finite elements used in this vibroacoustic problem is a method which directly treats the coupling between a structure and a fluid (light or heavy) and which is also well-adapted for such an LF and MF band. It does not need to extract the modal basis of the coupled fluid–structure system before calculating the responses. For more complex vibroacoustic systems having a true MF-behaviour, this method is more accurate than modal reduction methods. It is particularly well-adapted when frequency increases and/or modal densities of systems become large.

Acknowledgements

The authors would like to thank Dr. C. Soize of University of Marne-la-Vallée for the initiating of this research and his scientific support.

Appendix A. Formulation of the coupling between an acoustic bounded fluid and an elastic structure

We consider two coupled domains and we define: Ω is the bounded volume occupied by the internal fluid and Σ is its boundary, Ω_e is the elastic domain occupied by the structure of boundary Σ_e and Σ_F is a part of Ω_e where a set of loadings f_j^F is applied.

- The internal fluid is irrotational, viscous, compressible and its dynamics is defined by the internal pressure P. The fluid is given by its acoustical characteristics: mass density ρ_0, celerity of sound c_0 and dynamical viscosity η_0.

  The pressure P is usually defined from a velocity potential Φ as

$$P = -\rho_0 \frac{\partial \Phi}{\partial t}. \tag{A.1}$$

  (Φ is now the unknown variable to be found for acoustic fluid and it is scalar.)

  Introducing the linear operators $\mathbf{Q}$, $\mathbf{R}$ and $\mathbf{H}$, satisfying

$$\langle \mathbf{Q}\Phi, \phi \rangle = \frac{\rho_0}{c_0^2} \int_\Omega \Phi \cdot \phi \, \mathrm{d}x, \tag{A.2}$$

$$\langle \mathbf{R}\Phi, \phi \rangle = \rho_0 \int_\Omega \operatorname{grad} \Phi \cdot \operatorname{grad} \phi \, \mathrm{d}x, \tag{A.3}$$

$$\left\langle \mathbf{H}\phi, \frac{\partial \mathbf{u}}{\partial t} \right\rangle = \rho_0 \int_\Sigma \phi \left(\frac{\partial \mathbf{u}}{\partial t} \cdot n' \right) \mathrm{d}\sigma_\Sigma, \tag{A.4}$$

  the variational formulation in potential for the dynamics of the fluid becomes

$$\left\langle \mathbf{Q} \frac{\partial^2 \Phi}{\partial t^2}, \phi \right\rangle + \frac{4}{3} \frac{\eta_0}{\rho_0 c_0^2} \left\langle \mathbf{R} \frac{\partial \Phi}{\partial t}, \phi \right\rangle + \langle \mathbf{R}\Phi, \phi \rangle - \left\langle \mathbf{H}\phi, \frac{\partial \mathbf{u}}{\partial t} \right\rangle = 0, \tag{A.5}$$

where ϕ is a test admissible function and $\partial\mathbf{u}/\partial t$ the normal velocity of the structure over the interface Σ in direction n', where n' is the outgoing normal from Σ.

- Using for the structure the classical linear operators of mass $\mathbf{M}$, of damping $\mathbf{C}$ and of rigidity $\mathbf{K}$, the variational formulation for the dynamics of the elastic structure coupled to the internal fluid is

$$\left\langle \mathbf{M}\frac{\partial^2\mathbf{u}}{\partial t^2}, v \right\rangle + \left\langle \mathbf{C}\frac{\partial\mathbf{u}}{\partial t}, v \right\rangle + \langle \mathbf{Ku}, v\rangle + \left\langle \mathbf{H}\frac{\partial\Phi}{\partial t}, v \right\rangle = \langle \mathbf{G}, v\rangle, \tag{A.6}$$

where v is a displacement test admissible function and $\langle \mathbf{G}, v\rangle$ is defined by

$$\langle \mathbf{G}, v\rangle = \int_{\Sigma_F} f_j^F v_j \, \mathrm{d}S_{\Sigma_F}. \tag{A.7}$$

In Eqs. (A.5) and (A.6), $\mathbf{u} = (u_1, u_2, u_3)$ is the unknown displacement field of the structure to be found.

For the two coupled domains (fluid and structure), the weak formulation (coming from the combination of Eqs. (A.5) and (A.6) of the linear vibroacoustic problem to be solved is

$$\begin{bmatrix} \mathbf{M} & 0 \\ 0 & -\mathbf{Q} \end{bmatrix} \begin{pmatrix} \dfrac{\partial^2\mathbf{u}}{\partial t^2} \\ \dfrac{\partial^2\Phi}{\partial t^2} \end{pmatrix} + \begin{bmatrix} \mathbf{C} & \mathbf{H} \\ \mathbf{H}^t & -\dfrac{4}{3}\dfrac{\eta_0}{\rho_0 c_0^2}\mathbf{R} \end{bmatrix} \begin{pmatrix} \dfrac{\partial\mathbf{u}}{\partial t} \\ \dfrac{\partial\Phi}{\partial t} \end{pmatrix} + \begin{bmatrix} \mathbf{K} & 0 \\ 0 & -\mathbf{R} \end{bmatrix} \begin{pmatrix} \mathbf{u} \\ \Phi \end{pmatrix} = \begin{pmatrix} \mathbf{G} \\ 0 \end{pmatrix}. \tag{A.8}$$

Appendix B. Medium-frequency method developed at ONERA: "Onera-MF method"

This method is adapted to solve the following generic linear real matrices dynamical system coming from a finite element discretization, in a large band of frequency:

$$[-\omega^2\mathbf{M} + \mathrm{j}\omega\mathbf{C}(\omega) + \mathbf{K}(\omega)]\hat{\mathbf{u}}(\omega) = \hat{\mathbf{f}}(\omega). \tag{B.1}$$

$\mathbf{M}$, $\mathbf{C}(\omega)$, $\mathbf{K}(\omega)$, $\hat{\mathbf{u}}(\omega)$ and $\hat{\mathbf{f}}(\omega)$ are, respectively, the mass, damping and rigidity matrices, nodal displacements and forces vectors.

The "Onera-MF method" consists in dividing the MF broad band, denoted B, into several narrower frequency sub-bands, denoted B_n. Then $B = \bigcup_n B_n$.

Each sub-band B_n has a compact support and is defined by its central frequency ω_n and by its bandwidth $\Delta\omega$, through $B_n = [\omega_n - \Delta\omega/2, \omega_n + \Delta\omega/2]$ granting the condition $\Delta\omega/\omega_n \ll 1$.

For each B_n, three quantities are defined:

(1) $B_0 = [-\Delta\omega/2, \Delta\omega/2]$ is the LF-sub-band associated to the MF-sub-band B_n,
(2) $\tau_L = 2\pi/\Delta\omega$ is the *long time scale* and
(3) $\tau_S = 2\pi/\omega_n$ is the *short time scale*.

For $\omega \in B_n$, system (B.1) can be reduced to

$$[-\omega^2\mathbf{M} + \mathrm{j}\omega\mathbf{C}(\omega) + \mathbf{K}(\omega)]\hat{\mathbf{u}}_n(\omega) = \hat{\mathbf{f}}_n(\omega). \tag{B.2}$$

Because B_n is a narrow band, system (B.2) can be approximated by

$$[-\omega^2\mathbf{M} + \mathrm{j}\omega\mathbf{C}(\omega_n) + \mathbf{K}(\omega_n)]\hat{\mathbf{v}}_n(\omega) = \hat{\mathbf{f}}_n(\omega). \tag{B.3}$$

This new linear real matrices system is then solved in three steps:

(1) The short time scale τ_S which is associated to ω_n is analytically treated in the frequency domain using a frequency shift technique. This shift consists in assuming:

- $\omega = \omega' + \omega_n$. If $\omega \in B_n$ then $\omega' \in B_0$.
- $\mathbf{f}_0(t) = \mathbf{f}_n(t)\mathrm{e}^{-\mathrm{j}\omega_n t}$.
- $\mathbf{v}_0(t) = \mathbf{v}_n(t)\mathrm{e}^{-\mathrm{j}\omega_n t}$.

Fourier transform of the two equations above yields

$$\hat{\mathbf{v}}_0(\omega') = \hat{\mathbf{v}}_n(\omega' + \omega_n) = \hat{\mathbf{v}}_n(\omega), \tag{B.4}$$

$$\hat{\mathbf{f}}_0(\omega') = \hat{\mathbf{f}}_n(\omega' + \omega_n) = \hat{\mathbf{f}}_n(\omega). \tag{B.5}$$

Because B_n has a compact support, the support of solution $\hat{\mathbf{v}}_0(\omega')$ and external excitation $\hat{\mathbf{f}}_0(\omega')$ is sub-band B_0. From a practical point of view, we can define

$$\hat{\mathbf{f}}_0(\omega') = \begin{cases} 1 & \text{for } \omega' \in B_0, \\ 0 & \text{for } \omega' \notin B_0. \end{cases} \tag{B.6}$$

So, its inverse Fourier transform $\mathbf{f}_0(t)$ is the scalar cardinal sinus function, such as

$$\mathbf{f}_0(t) = \frac{1}{\pi t}\sin\left(\frac{t\Delta\omega}{2}\right) \tag{B.7}$$

which is defined over $]-\infty, +\infty[$.

This function tends rapidly to zero when t tends to $\pm\infty$ and the energy is concentrated around value $t = 0$.

We can see at this step of development that the MF-solution $\hat{\mathbf{v}}_n(\omega)$ in sub-band B_n can be deduced from its associated LF-solution $\hat{\mathbf{v}}_0(\omega')$ obtained in sub-band B_0.

Replacing ω by $\omega' + \omega_n$ and using Eqs. (B.4) and (B.5), the LF-equation associated to problem (B.3) to be solved in the frequency domain over sub-band B_0 is then

$$[-\omega'^2\mathbf{M}_n + \mathrm{j}\omega'\mathbf{C}_n + \mathbf{K}_n]\hat{\mathbf{v}}_0(\omega') = \hat{\mathbf{f}}_0(\omega'), \tag{B.8}$$

where

$$\begin{aligned} \mathbf{M}_n &= \mathbf{M}, \\ \mathbf{C}_n &= 2\mathrm{j}\omega_n\mathbf{M} + \mathbf{C}(\omega_n), \\ \mathbf{K}_n &= -\omega_n^2\mathbf{M} + \mathrm{j}\omega_n\mathbf{C}(\omega_n) + \mathbf{K}(\omega_n). \end{aligned} \tag{B.9}$$

Real matrices of system (B.3) have become now complex matrices.

For reasons of prohibitive numerical cost explained in Section 4.1.2, the above linear complex matrices system (B.8) is not solved by a direct frequency-by-frequency method in frequency domain but it is solved in time domain.

(2) Applying to this system the inverse Fourier transform with respect to ω', the LF equation in time domain which is associated to the long time scale τ_L to be solved over sub-band B_0 is

defined by

$$\mathbf{M}_n\ddot{\mathbf{v}}_0(t) + \mathbf{C}_n\dot{\mathbf{v}}_0(t) + \mathbf{K}_n\mathbf{v}_0(t) = \mathbf{f}_0(t). \tag{B.10}$$

This linear complex matrices system is then solved in the time domain by a step-by-step centred Newmark method of parameters $\alpha = 0.25$ and $\beta = 0.5$ which is unconditionally stable and where initial conditions are assumed to be zero. We define the following coefficients α_0, α_1, a_0, a_1 and a_2 due to the MF-algorithm by

$$\begin{aligned} &\alpha_0 = 4/\Delta t^2 + 4\mathrm{j}\omega_n/\Delta t, \quad \alpha_1 = 2/\Delta t, \\ &a_0 = 4/\Delta t^2 + 4\mathrm{j}\omega_n/\Delta t - \omega_n^2, \quad a_1 = 2/\Delta t + \mathrm{j}\omega_n, \quad a_2 = 4/\Delta t + 2\mathrm{j}\omega_n. \end{aligned} \tag{B.11}$$

If $\Delta t = t_{m+1} - t_m$ is the time-integration step of the scheme and $t_0 = 0$, the initial time, then the numerical Newmark scheme is defined by the following set of equations:

$$\mathbf{v}_0(t_0) = \{0\}, \quad \dot{\mathbf{v}}_0(t_0) = \{0\}, \quad \ddot{\mathbf{v}}_0(t_0) = \{0\}, \tag{B.12}$$

$$\ddot{\mathbf{v}}_0(t_{m+1}) = \frac{4}{\Delta t^2}\mathbf{v}_0(t_{m+1}) - \frac{4}{\Delta t^2}\mathbf{v}_0(t_m) - \frac{4}{\Delta t}\dot{\mathbf{v}}_0(t_m) - \ddot{\mathbf{v}}_0(t_m), \tag{B.13}$$

$$\dot{\mathbf{v}}_0(t_{m+1}) = \frac{2}{\Delta t}\mathbf{v}_0(t_{m+1}) - \frac{2}{\Delta t}\mathbf{v}_0(t_m) - \dot{\mathbf{v}}_0(t_m). \tag{B.14}$$

At step $m+1$, the solution of Eq. (B.10) $\mathbf{v}_0(t_{m+1}) = \mathbf{v}_0(m\Delta t)$ is obtained from the resolution of the next equation, with respect to the solution at step m:

$$\begin{aligned} [\mathbf{K}_n(\omega_n) + a_1\mathbf{C}_n(\omega_n) + a_0\mathbf{M}_n]\mathbf{v}_0(t_{m+1}) = \mathbf{f}_0(t_{m+1}) + \mathbf{M}_n[\alpha_0\mathbf{v}_0(t_m) + a_2\dot{\mathbf{v}}_0(t_m) + \ddot{\mathbf{v}}_0(t_m)] \\ + \mathbf{C}_n(\omega_n)[\alpha_1\mathbf{v}_0(t_m) + \dot{\mathbf{v}}_0(t_m)]. \end{aligned} \tag{B.15}$$

From the above solution of $\mathbf{v}_0(t_{m+1})$, we can then deduce solutions of $\ddot{\mathbf{v}}_0(t_{m+1})$ and $\dot{\mathbf{v}}_0(t_{m+1})$ with respect to solutions at step m using Eqs. (B.13) and (B.14).

To ensure the stability of Newmark scheme and the convergence of solutions of Eqs. (B.13)–(B.15), Δt must be chosen by

$$\Delta t = \tau_L/M_T, \quad \text{where } M_T \text{ is an integer which must be greater than 3.}$$

(3) The MF-solution $\hat{\mathbf{v}}_n(\omega)$ of system (B.3) for any discrete frequency of sub-band B_n is now built at a very small numerical cost from the LF-solutions of Eq. (B.15) only given at sampling time steps $\mathbf{v}_0(m\tau_L)$, by a Shannon transform.

The result of Shannon transform is

$$\hat{\mathbf{v}}_n(\omega) = \tau_L \sum_m \mathbf{v}_0(m\tau_L)\mathrm{e}^{-\mathrm{j}m\tau_L(\omega-\omega_n)}. \tag{B.16}$$

The above solution can easily be approximated by

$$\hat{\mathbf{v}}_n(\omega) \simeq \tau_L \sum_{m=-M_I}^{M_S} \mathbf{v}_0(m\tau_L)\mathrm{e}^{-\mathrm{j}m\tau_L(\omega-\omega_n)}. \tag{B.17}$$

M_I and M_S are, respectively, the starting and ending points of cardinal sinus function $\mathbf{f}_0(t)$ defined by (B.7) in Newmark scheme and in practice they are relatively small and this explains the numerical efficiency of the Onera–MF algorithm.

The real efficiency of the method comes from that Eq. (B.10) contains all the dynamics of the analyzed system over sub-band B_n and its resolution in time domain is performed only one time for each sub-band B_n at a much cheaper numerical cost than a direct frequency-by-frequency method which would need to inverse system (B.3) for a great number of frequencies belonging to B_n if we wanted to get the same frequency resolution as the one given by Eq. (B.17). The efficiency also comes from that Shannon Transform (B.16) gives a continuous spectrum of the frequency solution over sub-band B_n.

Appendix C. Analytical calculation of the vibroacoustic response of a parallelepipedic acoustic cavity filled with water and coupled to a four-edged clamped elastic plate

The mathematical developments presented in this appendix are based on considerations coming from the book [15, pp. 256–261] which deals with the vibroacoustics of a cylinder containing a fluid.

C.1. Dynamics of plate

According to Ref. [15], the displacement of the four-edged clamped elastic plate coupled to the internal fluid can be put in the form

$$w(x,y,\omega)=\sum_{m=2}^{+\infty}\sum_{n=2}^{+\infty}\frac{\boldsymbol{\phi}_{mn}(x,y)\int_S P(x,y,\omega)\boldsymbol{\phi}_{mn}(x,y)\,\mathrm{d}S}{m_s[\omega_{mn}^2-\omega^2+\mathrm{j}\eta_s\omega\omega_{mn}]\int_S \boldsymbol{\phi}_{mn}^2(x,y)\,\mathrm{d}S}, \tag{C.1}$$

where $m_s=\rho h$ is the mass of plate per unit area; S is the area of the plate; $\tilde{E}=E(1+\mathrm{j}\eta_s)$ is the complex Young modulus of plate; η_s is the mean damping loss factor of plate and

$$P(x,y,\omega)=F\delta(x_0,y_0)-p(x,y,0,\omega). \tag{C.2}$$

The eigenmodes $\boldsymbol{\phi}_{mn}$ and the eigenfrequencies ω_{mn} are issued from Ref. [1] for a four-edged clamped plate in which the eigenmodes are orthogonal. In Ref. [1], $\boldsymbol{\phi}_{mn}(x,y)=\boldsymbol{\phi}_m(x)\times\boldsymbol{\phi}_n(y)$. F is the one-point force applied at (x_0,y_0) and $p(x,y,0,\omega)$ is the solution of acoustic problem over surface of plate.

C.2. Acoustic problem for internal cavity

Acoustic problem inside cavity is:

$$\begin{aligned}&\Delta p+\tilde{k}^2p=0 \quad \text{in volume } \Sigma,\\ &\frac{\partial p}{\partial z}=\rho_0\omega^2 w \quad \text{over elastic plate},\\ &\frac{\partial p}{\partial \boldsymbol{n}}=0 \quad \text{over rigid faces.}\end{aligned} \tag{C.3}$$

$\tilde{k}$ is the complex acoustic wavenumber and by introducing the mean acoustic dissipation factor η_a inside cavity, $\tilde{k}$ can be put in the form:

$$\tilde{k}^2 = \frac{\omega^2}{c_0^2(1+\mathrm{j}\eta_a)} \simeq \frac{\omega^2}{c_0^2}(1-\mathrm{j}\eta_a) \quad \text{with } \eta_a = \frac{4}{3}\frac{\omega\eta_0}{\rho_0 c_0^2},$$

where $\eta_0 = 0.001$ is the dynamical viscosity of water.

We will find a solution of the internal pressure $p(x,y,z,\omega)$, satisfying boundary conditions on rigid faces, under the form

$$p(x,y,z,\omega) = \sum_{p=0}^{+\infty}\sum_{q=0}^{+\infty} P_{pq}(\omega)\cos(k_p x)\cos(k_q y)\{\mathrm{e}^{k_z(L_z-z)} + \mathrm{e}^{-k_z(L_z-z)}\} \tag{C.4}$$

with

$$k_p = \frac{p\pi}{L_x}, \quad k_q = \frac{q\pi}{L_y}, \quad k_z^2 = k_p^2 + k_q^2 - \frac{\omega^2}{c_0^2} + \mathrm{j}\frac{\eta_a\omega^2}{c_0^2} = (\alpha+\mathrm{j}\beta)^2.$$

The real and imaginary parts of wavenumber k_z are given by

$$\alpha = \left(\frac{k_{pq}^2 + \sqrt{k_{pq}^4 + \eta_a^2\dfrac{\omega^4}{c_0^4}}}{2}\right)^{1/2}, \quad \beta = \left(\frac{-k_{pq}^2 + \sqrt{k_{pq}^4 + \eta_a^2\dfrac{\omega^4}{c_0^4}}}{2}\right)^{1/2},$$

where

$$k_{pq}^2 = k_p^2 + k_q^2 - \frac{\omega^2}{c_0^2}.$$

Form (C.4) of $p(x,y,z,\omega)$ must also satisfying the boundary condition (C.3) over the elastic plate.

A combination of Eq. (C.1) providing displacement of plate and Eqs. (C.4) and (C.2) giving pressure restricted at surface of plate leads to the solution of the following linear system which is:

$$\begin{aligned} -\frac{1}{\rho_0\omega^2}\sum_{pq} P_{pq}(\omega)\cos(k_p x)\cos(k_q y)\,\mathrm{d}f_{pq} \\ = F\times\sum_{mn}\frac{\boldsymbol{\phi}_{mn}(x,y)\boldsymbol{\phi}_{mn}(x_0,y_0)}{B_{mn}(\omega)\int_S \boldsymbol{\phi}_{mn}^2(x,y)\,\mathrm{d}S} \\ -\sum_{pq} P_{pq}(\omega)\times f_{pq}\times\sum_{mn} Z_{mnpq}\frac{\boldsymbol{\phi}_{mn}(x,y)}{B_{mn}(\omega)\int_S \boldsymbol{\phi}_{mn}^2(x,y)\,\mathrm{d}S}, \end{aligned} \tag{C.5}$$

where

$$B_{mn}(\omega) = m_s[\omega_{mn}^2 - \omega^2 + \mathrm{j}\eta_s\omega\omega_{mn}],$$

$$Z_{mnpq} = \int_S \phi_{mn}(x,y)\cos(k_p x)\cos(k_q y)\,\mathrm{d}S = \int_0^{L_x} \phi_m(x)\cos(k_p x)\,\mathrm{d}x \cdot \int_0^{L_y} \phi_n(y)\cos(k_q y)\,\mathrm{d}y,$$

$$f_{pq} = \cos(\beta L_z)\cosh(\alpha L_z) + \mathrm{j}\sin(\beta L_z)\sinh(\alpha L_z),$$

$$\mathrm{d}f_{pq} = \alpha\cos(\beta L_z)\sinh(\alpha L_z) - \beta\sin(\beta L_z)\cosh(\alpha L_z) + \mathrm{j}[\beta\cos(\beta L_z)\sinh(\alpha L_z) + \alpha\sin(\beta L_z)\cosh(\alpha L_z)].$$

If the two members of Eq. (C.5) are multiplied by $\phi_{rs}(x,y)$, by integrating Eq. (C.5) over surface S of plate, orthogonality of modes ϕ_{mn} leads for any couple (r,s) to a set of coupled equations where variables $P_{pq}(\omega)$ are the unknown quantities to be found:

$$\sum_{pq} P_{pq}(\omega)\, Z_{rspq}\left\{f_{pq} - \frac{B_{rs}(\omega)}{\rho_0\omega^2}\,\mathrm{d}f_{pq}\right\} = F \times \phi_{rs}(x_0,y_0). \tag{C.6}$$

Finally, Eq. (C.4) gives the solution for $p(x,y,z,\omega)$ inside internal fluid and Eq. (C.1) and (C.2) for $w(x,y,\omega)$ of the plate.

References

[1] G.B. Warburton, The vibration of rectangular plates, Proceedings of the Institution of Mechanical Engineers 168 (1954) 371–381.

[2] M. Amabili, G. Delpiaz, Breathing vibrations of a horizontal circular cylindrical tank shell, partially filled with liquid, Transactions of American Society of Mechanical Engineers: Journal of Vibration and Acoustics 117 (2) (1995) 187–191.

[3] R.J. Allemang, D.L. Brown, A correlation coefficient for modal vector analysis, Proceedings of First International Modal Analysis Conference, Orlando, FL, 1982, pp. 110–116.

[4] C. Soize, Medium frequency linear vibrations of anisotropic elastic structures, La Recherche Aérospatiale 1982-5 (1982) 353–376.

[5] C. Soize, P.-M. Hutin, A. Desanti, J.-M. David, F. Chabas, Linear dynamic analysis of mechanical systems in the medium frequency range, Computers and Structures 23 (5) (1986) 605–637.

[6] C. Soize, A. Desanti, J.M. David, Numerical methods in elastoacousticity for low and medium frequency ranges, La Recherche Aérospatiale 1992-5 (1992) 25–44.

[7] H.-J.-P. Morand, R. Ohayon, Fluid Structure Interaction, Wiley, New York, 1995.

[8] M. Dussac, P. Martin, H.J. Marze, F. Chabas, J.M. David, A. Desanti, N. Meidinger, C. Soize, A finite element method to predict internal noise levels at discrete frequencies for a partially composite helicopter fuselage, AHS Annual Forum, Boston, MA, USA, 1989.

[9] C. Soize, J.M. David, A. Desanti, Dynamic and acoustic response of coupled structure/dense fluid axisymmetric systems excited by a random wall pressure field, La Recherche Aérospatiale 1989-5 (1989) 1–14.

[10] J.M. David, Vibroacoustics of a cylinder in air and in water. Prediction by numerical methods and statistical energy analysis and experimental comparisons, Third Colloque of GDR1138/Vibroacoustique, Le Mans, France, 1997.

[11] L. Guillaumie, J.M. David, O. Voisin-grall, Internal fuselage noise: comparison of computations and tests on a Falcon airframe, Aerospace Science and Technology 4 (8) (2000) 545–554.
[12] J.M. David, L. Guillaumie, Vibration and internal noise prediction of an aircraft fuselage in the low- and medium-frequency ranges, ISMA25 Congress, Leuven, Belgium, 2000.
[13] J.M. David, Internal noise prediction within aircrafts cabin in medium- and high-frequency domains, ICSV9 Congress on Sound and Vibration, Orlando, FL, USA, 2002.
[14] R. Ohayon, C. Soize, Structural Acoustics and Vibration, Academic Press, London–San Diego, 1998.
[15] C. Lesueur, Rayonnement Acoustique des Structures, Editions Eyrolles, Paris, 1988.